Full Length Article

Transient 3D simulations of turbulent premixed flames of gas-to-liquid (GTL) fuel in a fan-stirred combustion vessel

Abdellatif M. Sadeq, Samer F. Ahmed [*], Ahmad K. Sleiti

Mechanical and Industrial Engineering Department, College of Engineering, Qatar University, Doha P O Box 2713, Qatar

ABSTRACT

This work aims to conduct turbulent flame studies of GTL fuel and 50/50 diesel-GTLblend and compare them to diesel under a wide range of equivalence ratio ($0.7 < \Phi < 1.3$) and turbulence intensities (0.5 m/s < u′ < 3.0 m/s). For this purpose, Zimont Turbulent Flame Speed Closure (Zimont TFC) model is adapted and implemented into ANSYS Fluent to study the influence of turbulence on premixed combustion. The model is verified against the experimental results of the turbulent flame speeds for methane-air mixture using a cylindrical fan-stirred combustion vessel. Results show that (i) rich diesel and lean GTL fuels are characterized by a faster flame development and higher turbulent flame speeds; (ii) at the same elapsed time, Re_T and Da are found to be greater for stoichiometric GTL fuel compared to diesel and 50/50 diesel GTL blend, which indicates that the flame propagates towards the vessel's wall at a faster rate and the chemistry has dominated turbulence in a shorter time, and (iii) at low turbulence intensity level (u′=0.5 m/s), the flame morphology is defined by a wrinkled flamelet regime in Borghi diagram. However, at moderate and higher turbulence levels (u′=1.5 m/s and u′=3.0 m/s, respectively), the flame structure is defined by the corrugated flamelets regime. Furthermore, the turbulence homogeneity and isotropy have been investigated throughout the combustion vessel by conducting a study for the turbulent kinetic energy balance.

1. Introduction

The continuous fluctuation in oil prices and the increasing demand for clean fuels that can replace conventional fuels is a contemporary challenging issue. In addition, the increasing awareness about the harmful effect of greenhouse gases has directed the effort of researchers to find alternative energy resources that can substitute fossil fuels. In the past few decades, several research studies have been conducted to find alternative fuels that can enhance the engine performance and reduce the pollutant emissions at affordable prices [1–4]. Gas to Liquids (GTL) fuel is one alternative fuel that has gained much interest; especially in Qatar, Russia and the United States, in the recent years due to its many advantages [5]. One of these advantages is the clean burning nature of GTL that enhances the combustion properties when compared to crude-oil based diesel. Therefore, this fuel can reduce the exhaust emissions to meet the local and the international environmental regulations (The Paris Agreement, [6]). Moreover, GTL fuel is free of undesirable components such as metals, aromatics, and sulfur, which makes it less harmful to the environment with no toxicity. Furthermore, it is safer for storage and handling compared to diesel fuel and it does not have an

unpleasant smell [7]. According to Shell Company, GTL fuel can reduce Nitric Oxides emission by 25% and particulate matters emission by about 38% in comparison to diesel fuel [8]. This conclusion has been also confirmed by another research [9], which has further demonstrated that GTL fuel produces lower in-cylinder pressure and less brake specific fuel consumption. Due to these favorable GTL specifications and advantages, a systematic research needs to be conducted on the optimum combustion characteristics of GTL fuel at different operating conditions, and to determine its suitability for use in internal combustion engines. Detailed investigations for GTL combustion characteristics has not been performed yet, and it is essentially required before the start of using this alternative fuel widely in engines.

One of the experimental configurations that is extensively used to study the interaction between the flame propagation and turbulent eddies is the fan-stirred combustion vessel [9,10]. The homogeneous and isotropic turbulence can be generated inside the vessel using axisymmetric mixing fans mounted on the vessel's internal surface. This setup can be used at different thermodynamic conditions such as elevated temperatures, pressures, equivalence ratio and turbulence intensities, which are of vital significance for industrial applications [11,12]. The overall wrinkling rate of the flame surface and the

---

Nomenclature

Symbols

C	Reaction Progress Variable
C_p	Specific Heat at Constant Pressure, kJ/kg.K
Da	Damkohler Number
K	Thermal Conductivity, W/m.k
Ka	Karlovitz Number
k	Turbulent Kinetic Energy, m^2/s^2
Le	Lewis number
L_t	Integral Length Scale, m
n	Number of Product Species
P_o	Initial Pressure, atm
Re_T	Turbulent Reynolds Number
r	Vessel Radius, m
r_f	Flame Radius, m
r_{max}	Transition Radius, m
S_c	Reaction Progress Source Term, kg/m.s
S_{ct}	Turbulent Schmidt Number
S_l	Laminar Flame Speed, m/s
S_t	Turbulent Flame Speed, m/s
T_o	Initial Temperature, K
t_η	Kolmogorov Turbulence Time Scale, s
t_l	Characteristic Flame Time Scale, s
$\overline{U}$Mean	Velocity, m/s
u'	Turbulence Intensity, m/s
∇C	Progress Variable Gradient
Y_i	Mass Fraction of Product Species, i
$Y_{i, eq}$	Equilibrium Mass Fraction of Product Species, i

Greek letters

α	Thermal Diffusivity, m^2/s
Δ	Filter Size, m
Δt	Time Step Size, s
δ_l	Laminar Flame Thickness, m
δ_t	Turbulent Flame Brush Thickness, m
ε	Turbulence Dissipation Rate, m^2/s^3
μ	Dynamic Viscosity, $N.s/m^2$
ρ_b	Burned Mixture Density, kg/m^3
ρ_u	Unburned Mixture Density, kg/m^3
Σ	Flame Surface Density, m^{-1}
σ	Density Ratio
τ_c	Chemical Time Scale, s
τ_t	Turbulence Time Scale, s
ν	Kinematic viscosity, m^2/s
ν_η	Kolmogorov velocity, m/s
Φ	Equivalence Ratio

Abbreviations

CFD	Computational Fluid Dynamics
FSD	Flame Surface Density
GTL	Gas to Liquids
HIT	Homogeneous and Isotropic Turbulence
ID	Internal Diameter
IL	Internal Length
ISP	Intermediate Steady Propagation
LES	Large Eddy Simulation
OD	Outer Diameter
RANS	Reynolds Average Navier-Stokes
RMS	Root Mean Square
SGSF	Sub-Grid Scalar Flux
TFC	Turbulent Flame Speed Closure

turbulent burning velocity are highly dependent on the existing turbulence characteristics, such as the turbulent length scale, L_t and the turbulence intensity, u′. The initial flame kernel is small when compared to the integral length scale, and therefore it is not exposed to the full spectrum of turbulence during the early stage of flame development after ignition and it remains laminar. As the flame grows, the surface of the flame is wrinkled by larger energy containing eddies resulting in more energy and mass transfer, and a thickening in the flame surface. Consequently, a deep characterization of the turbulent flow is considered as a prerequisite to understand and analyze the flame-turbulence interaction within this setup. Although many researchers have experimentally used this setup to study the turbulent flow field, for example [13–22], the velocities of the flow can only be measured in a two-dimensional plane with limited resolutions and ranges, so that the spatial and temporal fluctuations of small-scale motions cannot be properly captured [23]. Hence, well verified and validated 3-D numerical simulations can bridge this gap.

There are several combustion models found in the literature, which are used primarily for modelling reactive flow behavior. One of these widely-used computational models for studying premixed turbulent combustion at high Reynolds numbers is the Zimont Turbulent Flame Speed Closure (TFC) model available in ANSYS Fluent, and implemented using the pressure-based solver algorithm [24,25]. In this model, the combustion process is described by a single transport equation (C-equation) for a progress variable C; turbulent closure for the progress variable's source term that depends on a model parameter used for turbulent flame speed computation. Particularly, phenomena like wrinkling, thickening, and straining of the flame front by the turbulent flow field are considered, resulting in a closed form expression of the turbulent flame speed, which involves critical gradient of the laminar flame thickness and speed, fluctuation intensity and the local turbulent length scale. This closure approach is very elegant and efficient, as it requires only one more transport equation compared to non-reacting flow case, in addition to excluding any costly evaluation of the chemical source terms or integration over probability density functions [26].

The TFC model has been implemented in a finite-volume-based fluid dynamics code and then validated against experimental data obtained from a large-scale gas turbine burner stand [25]. The computational results compared well to the experimental ones, and it has been noticed that this model is computationally more efficient when compared to other numerical models such as Flame Surface Density (FSD) model or Sub-Grid Scalar Flux (SGSF) model [25]. The FSD model should satisfy the realizability requirement that the flame surface density (Σ) must be always equal to or larger than the progress variable gradient (∇C), however this criterion is not satisfied at all flow conditions. Moreover, this model requires that the modelled local flame thickness has a size in the order of the filer size (Δ) to resolve the shape of the turbulent brush profile, i.e. a minimum number of computational grid points is numerically required within the modelled flame thickness, which raises the computational cost of the problem [27] . On the other hand, the use of SGSF model is found to have anisotropy and numerical instabilities when predicting the kinetic energy and scalar variance for wall bounded flows [28]. The use of Zimont model overcomes these difficulties, which makes it extremely interesting and suitable for applications of large three-dimensional, complicated geometries [29]. Besides, the Zimont TFC model has been validated for use in different configurations e.g., stationary flames [30], highly turbulent confined bluff-body flame [31], Bunsen flame [32] , turbulent V-flames [33], statistically spherical expanding flames in a fan-stirred vessel [34,35]and swirling premixed turbulent flames [36,37]. Some of these cases have been implemented

Table 1

Properties of diesel, GTL and 50/50 diesel-GTL blend [9]

Properties	Diesel	GTL	50/50 Diesel-GTL Blend
H/C Ratio	2.125	2.1–2.15	2.138
Approx. Formula	$C_{16}H_{34}$	$C_{16}H_{34}$	$C_{16}H_{34}$
Density at 15 °C (Kg/m^3)	866	760	813
Flash Point (°C)	55	77	66
Cetane No.	55	70	62.5
Calorific Value (MJ/kg)	44.3	47.3	45.8
Viscosity at 40 °C (mm^2/s)	5.2	2.0	3.6
Distillation Temperature (°C)	190–200	190	195

Table 2

Geometrical specifications and operating conditions for Texas A&M and QU vessel.

Vessel Name	Texas A&M Vessel [20]	QU Vessel [53]
Geometrical Specifications		
Vessel Shape	Cylindrical	Cylindrical
Internal Diameter (ID in cm)	30.5	40.0
Internal Length (IL in cm)	35.6	65.0
No. of Fans	4	4
No. of Blades of Each Fan	3	8
Fans Outer Diameter (OD in cm)	7.62	8.00
Pitch Angle (Degrees)	20	60
Operating Conditions		
Initial Temperature (T_o in K)	298	463
Initial Pressure (P_o in atm)	1	1
Equivalence Ratio (Φ)	0.7–1.3	0.7–1.3
Turbulence Intensity (u' in m/s)	0.85–1.30	0.50–3.00
Integral Length Scale (L_t in mm)	27	20
Fuel	Methane	Diesel, GTL, 50/50 diesel-GTL blend

using Large Eddy Simulation (LES) approach [38–41], while other have been performed using Reynolds Average Navier-Stokes (RANS) approach [42–44]. Furthermore, the model has been used with different fuels e.g., propane/butane [45], methane [46–48], and hydrogen [49].

Zimont TFC model was developed in 1979, and it can be implemented through a RANS or LES approach as mentioned above [50]. In order to effectively account for the turbulent viscosity, turbulence dissipation rate, vorticity and the chaotic behavior in the turbulent flow field, a realizable k- ε model is used in this research study to obtain the numerical solution along with an enhanced wall treatment [51]. According to Zimont [25], this model behaves effectively when any of the following physical mechanisms exist, (i) a gradual increase in the average propagating flame thickness, which can be interpreted by the turbulent diffusion's law [52], (ii) flame distortion by large scale vortices and broadening of local reaction zones by the effect of small-scale eddies, (iii) preferential diffusion of oxidizer or fuel into curved local reaction zones. All these mechanisms exist in the research problem at hand and hence in the present research study, the numerical solutions are obtained using Zimont TFC model for predicting the flame propagation, however without considering any interaction between the flame and the vessel's wall, because the flame-turbulence interaction is analyzed up to a vessel radius equals to 12 cm.

To summarize, this model has been selected for use rather than other numerical models due to the following reasons, (i) this model has been validated for various cases using several configurations and different types of fuels, therefore it can be used with a high reliability, (ii) the physical mechanisms encountered in this computational study can be effectively analyzed and resolved using Zimont TFC model, and (iii) this research aims to investigate turbulent flame speeds at high Reynolds numbers and Damkohler numbers, and as such, Zimont TFC model is suitable for use at these conditions.

The main objective of the current research is to perform detailed turbulent flame studies on pure GTL, 50/50 diesel-GTL blend, and compare them to pure diesel using Zimont TFC numerical model. The main knowledge gaps in open literature that the present study is targeting include: (i) investigating the existence of a homogenous and isotropic turbulent flow field throughout the combustion vessel by implementing a validated and verified numerical scheme, (ii) characterizing and analyzing the turbulent flame speeds for the three fuels at a broad range of turbulence intensities, equivalence ratio, Reynolds numbers and Damkohler numbers that are not studied before.

This study is presented in five major sections. In to the introduction section above, section 2 presents the experimental data used for Zimont TFC model validation, and for studying the premixed turbulent combustion of the investigated fuels including the geometrical specifications and operating conditions. Section 3 introduces the numerical simulation approach and section 4 presents the results of model validation. The results of this study are presented and discussed in section 5.

2. Experimental data for validation

In this research study, two cylindrical fan-stirred combustion vessels are modelled. The first one is the Texas A&M vessel, which is used for model validation through the comparison of the numerically computed methane-air turbulent flame speeds with the experimental ones [20]. The other one is Qatar University vessel, which is used for studying the premixed turbulent combustion of the three liquid fuel blends (diesel, GTL, 50/50 diesel-GTL blend). Table 1 lists the chemical and physical properties for diesel, GTL and 50/50 diesel-GTL blend [9]. This vessel has been designed at Qatar University in 2012, and it has been used for obtaining the laminar flame speeds for the three liquid fuel blends in 2016 [53]. Therefore, it is modelled in this study to compute the turbulent flame speeds for the three liquid fuels at different turbulent intensities and equivalence ratio. For simplicity, the name "QU vessel" is used in this research to indicate for the use of Qatar University combustion vessel. Table 2 summarizes the geometrical specifications and operating conditions for the two vessels.

3. Numerical simulation approach

In this section, the physical significance of Zimont TFC model is described in subsection 3.1, and the model's governing equations are presented in subsection 3.2. The numerical grid details and the complete description of the meshing process are handled in subsection 3.3. Finally, the numerical schemes, boundary conditions, physical constraints and the solution initialization are presented in subsection 3.4.

3.1. Model description

Zimont [24] proposed a model to solve the turbulent premixed flames by solving Favre averaged equation for the mean reaction progress variable C. The development of this model is based on a theoretical study that the turbulent flame moves with a steady propagation velocity that depends on the mixture's physico-chemical properties and on the surrounding turbulence effect [26]. In this model, combustion takes place in a thin and strongly wrinkled flame sheet that separates the reactants and the products. Thus, this model considers the division of the reacting flow field into regions of unburnt and burnt species, separated by the thin flame sheet that is propagating with a speed called the turbulent flame speed, S_t. Also, in this model, an averaged flame front is
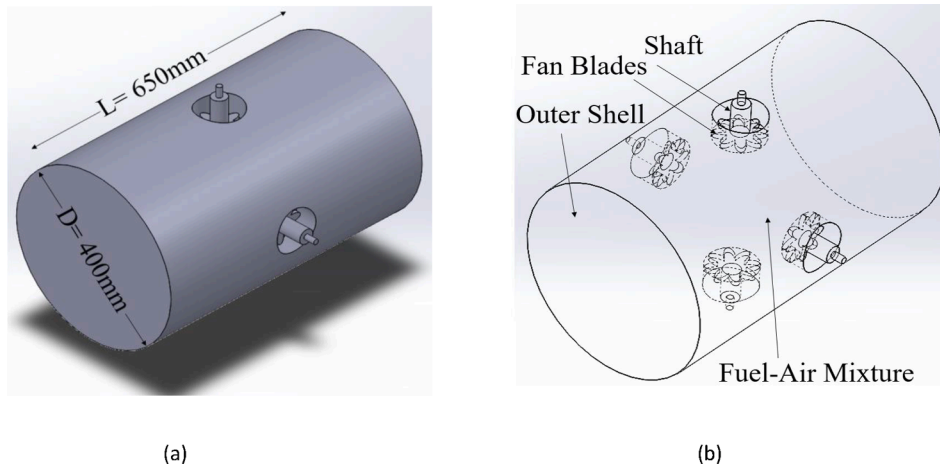
Fig. 1. (a) QU vessel's SOLIDWORK model with basic geometrical dimensions, (b) Schematic diagram that shows the component of QU vessel model.

tracked out instead of the exact one. Upon averaging, a region with an instantaneous realization of the flame might be found, and it will be surrounding the mean flame front. The region's width is known as the turbulent flame brush thickness δ_t. According to turbulent diffusion law [24], this model assumes an increasing thickness of the flame brush and a constant combustion velocity. Flames following these behaviors are known as intermediate steady propagation (ISP) flames. This further confirms the suitability of Zimont TFC model to handle the current ISP flames as it is valid for $Re_T \gg 1$, $Da \gg 1$ and $u \gg S_l$, where S_l is the laminar flame speed.

3.2. Governing equations

The flame front propagation is modelled by solving the transport equation of the density-weighted mean reaction progress variable, C [24,53,55]:

$$\frac{\partial}{\partial t}(\rho C) + \nabla.(\rho \overrightarrow{v} C) = \nabla.\left(\frac{\mu_t}{S_{ct}}\nabla C\right) + \rho S_c \quad (1)$$

where ρ is the fuel density, C is the mean reaction progress variable, S_{ct} is the turbulent Schmidt number, μ_t is the turbulent viscosity, and S_c is the reaction progress source term.

The reaction progress variable is defined as a normalized sum of the products species:

$$C = \frac{\sum_{i=1}^{n} Y_i}{\sum_{i=1}^{n} Y_{i,eq}} \quad (2)$$

where n is the number of product species, Y_i is the mass fraction of product species i, and $Y_{i,eq}$ is the equilibrium mass fraction of product species i.

According to this definition, C = 1 when the mixture is burned and C = 0 when the mixture is unburned. The value of C is used as a boundary condition at all flow inlets. It is either specified as C = 0 (unburned) or C = 1 (burned).

The mean reaction rate in equation (1) is modelled as:

$$\rho S_c = \rho_u S_t |\nabla C| \quad (3)$$

where ρ_u is the unburnt mixture density, and S_t is the turbulent flame speed.

The turbulent flame speed normal to the flame surface is influenced by the laminar flame speed, and the flame front is wrinkled and stretched by larger eddies. The Zimont turbulent flame speed closure computes S_t according the following equation:

$$S_t = A(u')^{0.75} S_l^{0.5} \alpha^{-0.25} L_t^{0.25} = Au'\left(\frac{\tau_t}{\tau_c}\right)^{0.25} \quad (4)$$

where A is a model constant, u' is the RMS (root mean square) velocity (m/s), S_l is the laminar flame speed (m/s), $\alpha = \frac{K}{\rho c_p}$ is the thermal diffusivity (m^2/s), L_t is the turbulence integral length scale (m), $\tau_t = \frac{l_t}{u'}$ is the turbulence time scale (s), and $\tau_c = \frac{\alpha}{S_l^2}$ is the chemical time scale (s)

The turbulent kinetic energy, k is computed from

$$k = \frac{3}{2}u'^2 \quad (5)$$

The turbulence integral length scale, L_t, is computed from

$$L_t = C_D\frac{(u')^3}{\varepsilon} \quad (6)$$

where ε is the turbulence dissipation rate, and C_D is a model constant.

This model assumes that the equilibrium small-scale eddies acts on the laminar flame and results in a turbulent flame speed formula that is completely defined by large-scale turbulent eddies. It is recommended to use the default value of 0.52 for A and the value of 0.37 for C_D, which are suitable for most premixed flames [55].

The model becomes specifically applicable when the Kolmogorov scales (e.g., the smallest turbulent eddies in the flow) are smaller than the laminar flame thickness and can penetrate the flame zone, which is known as the thin reaction zone combustion regime. This regime can be quantified using the Karlovitz number, Ka, which is defined as,

$$ka = \frac{t_l}{t_\eta} = \frac{\nu_\eta^2}{S_l^2} \quad (7)$$

where t_l is the characteristic flame time scale, t_η is the Kolmogorov (smallest) turbulence time scale, $\nu_\eta = (\nu\varepsilon)^{0.25}$ is the Kolmogorov velocity, and ν is the Kinematic viscosity.

Finally, it should be mentioned that this model is only applicable for the cases where the width of the flame brush expands with time, which is encountered in most industrial systems. Flames that propagate for an extended time reach a constant flame width, which contradicts the physical principles found in this model.

3.3. Numerical grid details

The geometrical domain of the problem consists of a cylindrical; steel vessel with a diameter of 40 cm and a volume of 81.7L. Two optical glass windows are installed on the vessel's outer shell for tracking the flame propagation using Schlieren photography. Four fans are installed on the
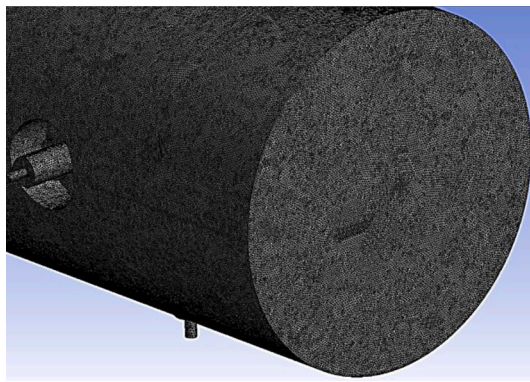
(a)
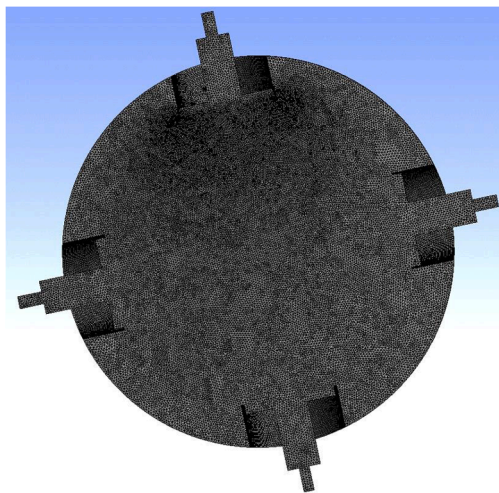
(b)

Fig. 2. (a) Meshed geometry, (b) Cross-section view for the mesh at the central circumference of the combustion vessel.

vessel's inner wall, which are located at the vessel's central circumference with an equal distance from each other. The fan's axes are oriented collinearly with the central point of the vessel, aiming to generate a homogeneous and isotropic turbulence flow field inside the vessel. The axial distance between one fan and the opposite one is 30 cm. Each fan has an outer diameter of 8 cm and consists of eight blades of 3.5 cm length each, and a pitch angle of 60^0. The complete description of the test rig can be found in Ref.[53].

The computational domain covers the whole vessel's internal volume that is approximated by a cylinder with four fans mounted on the vessel's wall. The combustion vessel model was designed using SOLID-WORKS 2020 and then exported to ANSYS Fluent 17.0 to generate the mesh [54]. Fig. 1(a) shows the model's geometry with basic dimensions, and Fig. 1(b) describes its main components.

Tetrahedral, quasi-equidistant elements are used to build the computational domain, using an adaptive size function, where each element has a size of 2 mm. A total number of 7.8 million cells were used to build up the computational mesh domain. Fig. 2(a) shows the meshed geometry, and Fig. 2(b) illustrates a cross-section view for the mesh at the central circumference of the combustion vessel.

The grid size is determined based on a grid detailed independence study, which is discussed in the subsequent sections. The numerical cells were ensured to be equally spaced by specifying the size function to be adaptive. The relevance Center (or resolution), which defines the middle

Table 3
Mesh details and statistics.

Size function	Adaptive
Relevance center	Fine
Smoothing	Medium
Span Angle Center	Fine
Element Size (mm)	2.00
Minimum Edge Length (mm)	0.59
Inflation Option	Smooth Transition
Nodes	1,422,642
Elements	7,844,078
Average Element Quality	0.84
Average Skewness	0.22
Orthogonal Quality	0.86

Table 4
Numerical model settings of the spark plug.

Processor Option	Serial
Solver Type	Pressure-Based
Velocity Formulation	Absolute
Time	Transient
Discretization	2nd Order Upwind
Species Model	Premixed Combustion Model
Flame Speed Model	Zimont Model
Viscous Model	K-epsilon, Realizable with Enhanced Wall Treatment
Premixed Charge	Diesel, GTL, 50/50 Diesel-GTL Blend (Methane Used for Validation Case)
Equivalence Ratio (Ø)	0.7 to 1.3
Spark Location	At the Center of the Vessel
Spark Energy (mJ)	40
Spark Duration (s)	0.0001
Spark's Transition Radius (mm)	0.5

point of the "Relevance" slider control was set to be fine for achieving a more stable solution. The smoothing option aims to improve the quality of meshing by moving the locations of nodes with respect to surrounding elements and nodes, and it was set to be "Medium". The use of a cylindrical geometry with a high curvature suggested the use of a fine span angle center in order for the meshed elements to precisely span the curvature angle. A fine span angle center ranges between $12°$ to 36^0 [56]. Table 3 summarizes the mesh details used throughout this numerical study.

3.4. Numerical model Settings, discretization and initialization

Zimont TFC model has been selected in this research study to investigate the flame propagation, and to obtain the turbulent flame speeds of the three liquid fuel blends (diesel, GTL, 50/50 diesel-GTL blend) at different equivalence ratio (Ø=0.7 to 1.3) and turbulence intensities (u′= 0.5 m/s to 3.0 m/s). The second order upwind has been selected as the discretization scheme; to ensure the convergence of the solution with a high accuracy and with an insensitivity to grid size variation.

Table 5
Solution initialization.

Solution Scheme	Coupled
Solution Initialization	Standard
Initial Pressure (atm)	1
Initial Temperature (K)	463
Integral Length Scale, L_t (mm)	20
Reaction Progress Variable, C at t = 0 s	Zero (at All Zones)
Time Step Size (s)	0.00025
Number of Time Steps	120
Maximum Iterations/Time Step	25

Table 6
Turbulence initial conditions for the validation cases.

Fan Speed (RPM)	Turbulence Intensity, u'(m/s)	Turbulent Kinetic Energy, $k(m^2/s^2)$	Turbulence Dissipation Rate, $\varepsilon(m^2/s^3)$
8000	0.85	1.08	8.42
11,200	0.90	1.22	9.99
14,400	1.00	1.50	13.70
17,600	1.10	1.82	18.24
20,800	1.20	2.16	23.68
24,000	1.30	2.54	30.11

Unlike the segregated pressure base algorithm, the coupled algorithm solves a system of continuity and momentum equations simultaneously; subsequently this results in a faster solution convergence while consuming a larger memory size. As this study comprises a large number of results, this algorithm has been selected for use. According to the literature review, many studies have considered running the turbulent flame speed experiment using integral length scale, L_t = 20 mm [13,20,57–59], therefore this value is used in the solution initialization to obtain the turbulence dissipation rate in equation (6).

Moreover, it should be noticed that a value of C = 0 must be used in the solution initialization to indicate unburnt mixture prior to the ignition. A spark plug with a 40 mJ energy is placed in the center of the combustion vessel, where the flame kernel initiates and starts to propagate spherically in all directions. Table 4 lists the details of the used numerical models and spark plug, and Table 5 lists all the information used in the settings of the solution initialization.

4. Model validation

To validate and demonstrate the validity of using Zimont TFC model to predict turbulent flame propagation, the case of cylindrical combustion vessels is considered. In this validation, turbulent flame speeds are computed for a fully premixed methane-air mixture and compared to the experimental ones found in the work of Ravi [20]. The successful validation of this numerical model will allow using it in studying the premixed turbulent combustion of diesel, GTL and 50/50 diesel-GTL blend inside the cylindrical combustion vessel. The numerical scheme followed to perform the computational fluid dynamics (CFD) calculations is described in subsection 4.1. After that, the results are presented in subsection 4.2 through performing a grid independency study.

4.1. CFD solution method

Turbulent flame speeds experiments that were performed for methane-air mixture using Texas A&M vessel [20] are used for comparison with CFD results. The geometrical specifications and operating conditions for the experiment are listed in Table 2, and the solver details are listed in Table 4 above. Tetrahedral, quasi-equidistant elements have been used to mesh the computational domain, using an adaptive size function, where each element has a size of 2 mm. A total number of 2.8 million cells were used to build up the computational mesh domain. Burned and unburned density, thermal conductivity, specific heat, molecular weight, viscosity, and the laminar flame speeds have been formulated as constants. The Laminar flame speed readings at the corresponding equivalence ratio have been extracted from the same experimental work [20]. A spark plug with a 40 mJ energy is placed in the center of the combustion vessel to ensure the ignition of the flammable mixture, where the flame kernel initiates and starts to propagate spherically in all the directions [60]. The experiment has been conducted under atmospheric pressure at an initial temperature of 298 K. Turbulent kinetic energy and turbulent dissipation rate at the corresponding turbulence intensities were obtained using equations (5) and (6), respectively. Table 6 summarizes all the test points used in this validation case.

4.2. Validation results

The methodology followed to validate the model and to present the results comprises a grid independency study, a time-step independency study and finally using the correct grid and time step size to conduct the full-validation study. For this case, three structured grids of different mesh sizes, each with tetrahedral cells were used to perform the mesh sensitivity study in the proposed geometry. Table 7 summarizes all the details of Grid I, II and III.

Turbulent flame speed results at different turbulence intensities are shown in Fig. 3(a). The results indicate that Grid I give mesh independency only at high turbulence intensities ($u' > 1.0$ m/s). However, at lower turbulence intensities, Grid I fails to capture the precise value of the turbulence flame speed. On the other hand, Grid II is found to be sufficient to give a grid independent solution at all turbulence intensities with an average relative error percentage of 3%. At low level of u', the flame brush thickness becomes thinner according to turbulent diffusion law explained by Zimont [52]. Consequently, more flame grid points are required to resolve the flame. As u' increases, the thickness of the flame brush becomes thicker and thus, the flame can be resolved using the same grid size. As Grid II provides a grid-independent solution, it can be then further used to conduct a time-step independency analysis.

Three different time step sizes have been used to demonstrate a time-step independent solution ($\Delta t = 2.5*10^{-4}$ s, $1.5*10^{-4}$ s and $5.0*10^{-5}$ s). As seen from the plot in Fig. 3(b), the results are independent of all the used time step sizes, which indicates that the use of a time-step $\Delta t = 2.5*10^{-4}$ s is fine enough for achieving a converged and stable solution. Based on this conclusion, a grid size of 2 mm and a time step of $\Delta t = 2.5*10^{-4}$ s will be used in the coming full validation.

The study of the flame ignition region that is located at the center of the vessel, and which is identified by the small transition radius (r_{max}) is an important parameter when performing premixed turbulent combustion calculations. This can be interpreted by the large augmentation of the flame speed at large values of r_{max}. Therefore, calculations with using different sizes of r_{max} were performed to check for the sensitivity of
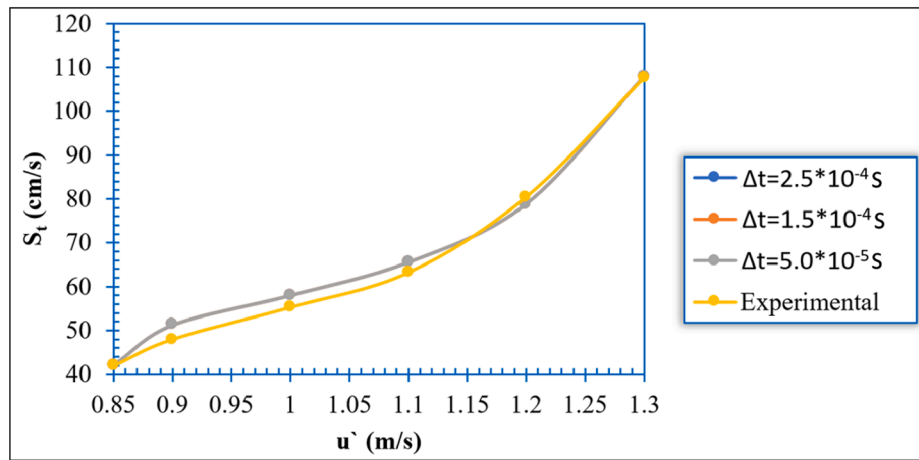
Table 7
Grids used to perform the mesh sensitivity study for the validation case. The relative error percentage is computed by comparing CFD results with the experimental work [20].

Grid No.	Element Size (mm)	No# Elements	No# Nodes	Turbulence Intensity, u'(m/s)					
				0.85	0.90	1.00	1.10	1.20	1.30
				S_t (cm/s)					
Grid I	3.00	1,136,343	213,452	43.64	52.89	58.90	66.08	79.04	108.02
% Relative error				3.90	10.14	6.48	4.54	1.76	0.40
Grid II	2.00	2,793,222	518,912	42.15	51.24	58.00	65.55	78.87	107.90
% Relative error				0.36	6.71	4.86	3.71	1.97	0.29
Grid III	1.00	17,702,581	3,164,221	42.10	51.19	57.85	65.45	78.82	107.88
% Relative error				0.24	6.60	4.59	3.55	2.03	0.27
Experimental [20]				42.00	48.01	55.31	63.21	80.45	107.59
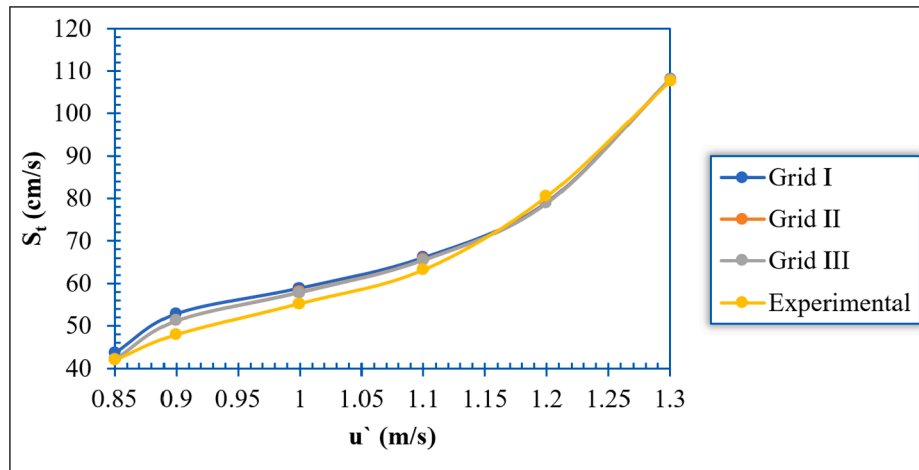
(a)

(b)
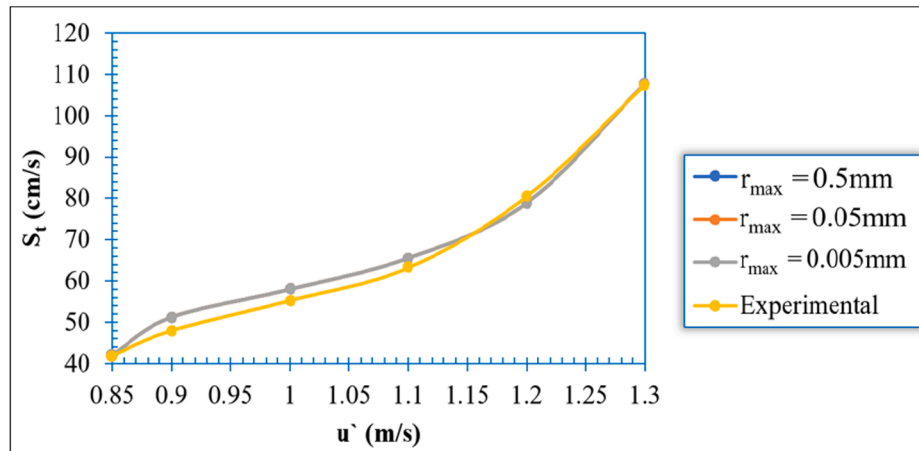
(c)

Fig. 3. (a) Grid independency results for the validation case, (b) Time-step independency results for the validation case, (c) Final geometry validation results using different ignition region sizes.

Table 8
Properties of the flames studied in the present work.

Fuel	Diesel	GTL	50/50 Blend
Property	$\Phi = 0.7$		
Laminar Flame Speed, S_l (cm/s)	42.88	55.88	50.43
Laminar Flame Thickness, δ_l (cm)	0.047	0.042	0.043
Density Ratio, σ	0.232	0.226	0.229
Reynolds Number, Re	480.2	519.0	513.2
Lewis Number, Le	1.204	0.988	1.096
Property	$\Phi = 1.0$		
Laminar Flame Speed, S_l (cm/s)	80.24	85.49	81.55
Laminar Flame Thickness, δ_l (cm)	0.034	0.033	0.033
Density Ratio, σ	0.194	0.186	0.190
Reynolds Number, Re	571.4	528.0	534.5
Lewis number, Le	1.039	0.985	1.012
Property	$\Phi = 1.3$		
Laminar Flame Speed, S_l (cm/s)	78.78	82.17	79.04
Laminar Flame Thickness, δ_l (cm)	0.027	0.030	0.029
Density Ratio, σ	0.201	0.210	0.206
Reynolds Number, Re	406.9	392.5	398.4
Lewis number, Le	0.947	1.138	1.042

Table 9
Turbulence initial conditions studied in the present work.

Fan Speed (RPM)	Turbulence Intensity, u' (m/s)	Turbulent Kinetic Energy, k (m²/s²)	Turbulence Dissipation Rate, ε(m²/s³)
7000	0.50	0.38	2.31
9800	1.00	1.50	18.50
11,600	1.50	3.38	62.40
14,400	2.00	6.00	148.00
17,200	2.50	9.38	289.10
21,000	3.00	13.50	499.50

the computed results to variations in the transition radius size. Turbulent flame speeds at three different values of r_{max} were computed, as shown in Fig. 3(c). It can be clearly noticed that the results are independent of all the used transition radius sizes, which indicates that the use of $r_{max} = 0.5$ mm is fine enough to reach a converged solution.

5. Results and discussions

In this section, the results of turbulent flame studies conducted on the three investigated liquid fuel blends (diesel, pure GTL, 50/50 diesel-GTL blend) are presented in five categories; (5.1) mean turbulent kinetic energy balance, (5.2) flame radius evolution, (5.3) turbulent flame speeds, S_t, (5.4) dimensionless numbers for turbulent combustion, (5.5) Borghi diagram. The mixture properties and the laminar flame parameters were estimated using GASEQ and PREMIX program available in CHEMKIN-PRO [61,62]. The PREMIX program obtains the thermodynamics, kinetic and transport parameters through accessing TRASPORT and CHEKIN Gas-phase packages. Therefore, the flame problem is solved by initially executing the two preprocessor programs, "tran" and "chem", which have an access to transport and thermodynamic property databases in CHEMKIN-PRO [63]. Mixture properties such as burned and unburned density, thermal conductivity, specific heat, molecular weight, viscosity, and the laminar flame speeds have been formulated as constants in ANSYS Fluent. Although lean combustion ($\Phi < 1.0$) is practically used in diesel engines to reduce Nitrogen Oxides emissions, this study aims to investigate the premixed turbulent combustion at a wide range of flammability ($0.7 < \Phi < 1.3$) to characterize the behavior of the flame at different operating conditions. In addition, many reviews considered the use of this range of equivalence ratios in their premixed laminar or turbulent combustion studies [21,22,62,66]. Table 8 lists the major flame parameters related to this study. In addition, it should be mentioned that the results of this study have been smoothed and filtered out, allowing the important patterns to stand out.

The simulation has been conducted under atmospheric pressure at an initial temperature of 463 K. Initial turbulent velocities were varied by changing fan's speeds. Turbulent kinetic energy and turbulent dissipation rate at the corresponding turbulence intensities were obtained using equations (5) and (6), respectively. Table 9 lists all the turbulence initial conditions used in this study.
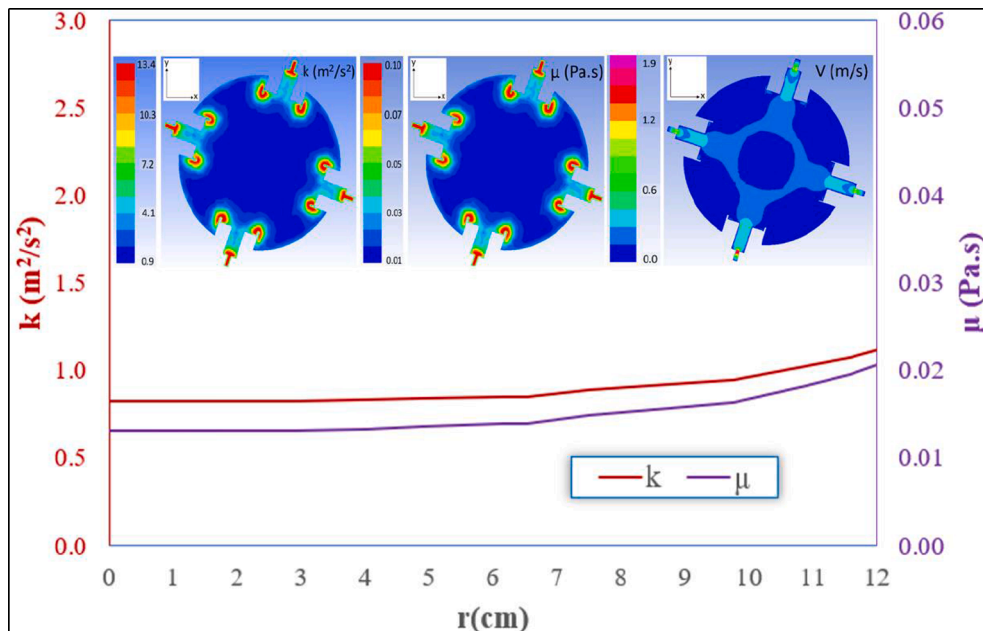

Fig. 4. Mean turbulent kinetic energy and turbulent eddy viscosity throughout the combustion vessel up to r = 12 cm, at u'=3.0 m/s and $\Phi = 1.0$.
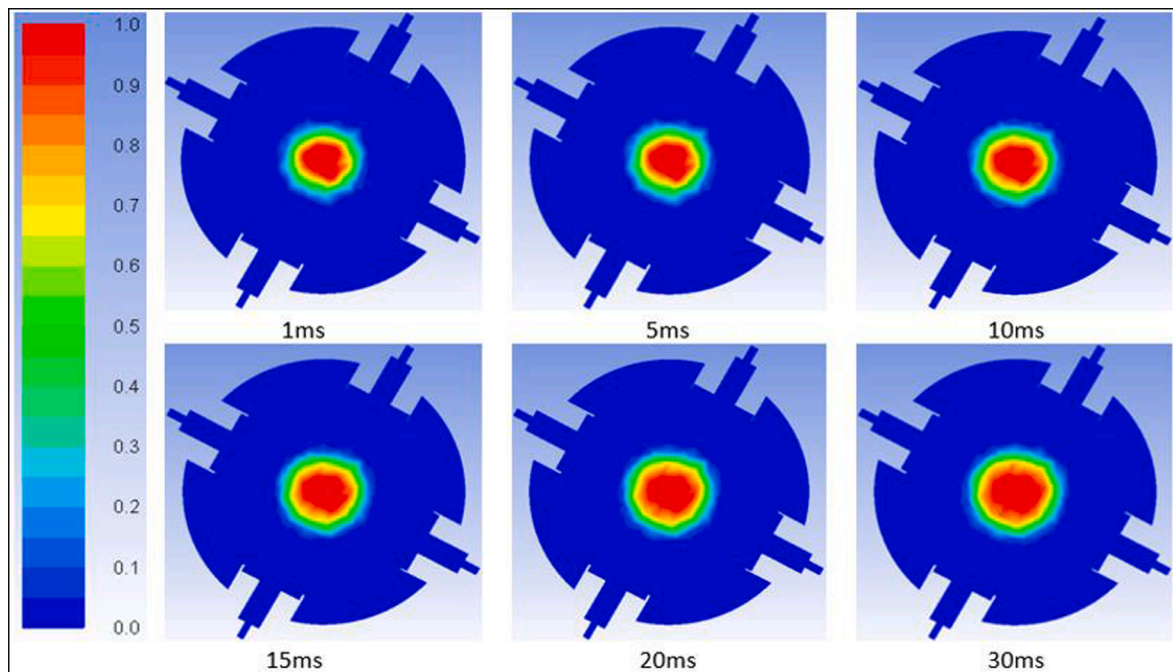
Fig. 5. Flame radius evolution for stoichiometric GTL-air mixture at 1 atm and u′=3.0 m/s.

5.1. Mean turbulent kinetic energy balance

The objective of studying the mean turbulent kinetic energy balance; is to show how the turbulence generated in the fan's region is transferred to the center of the vessel. Turbulence is characterized by its dissipative nature; in which the flow's turbulent kinetic energy is converted into an internal energy due to eddy viscosity, which is also known as the energy cascade theorem [65]. A relevant quantity used to characterize the turbulence inside the vessel in terms of dissipation, production and transport is the mean turbulent kinetic energy. In addition, studying this quantity ensures the existence of HIT (Homogeneous and Isotropic Turbulence) in the center of the vessel. Besides, analyzing the attitude of this quantity prior to ignition assists in selecting a suitable flame radius at which the computational results will be obtained [66]. The mean turbulent kinetic energy and turbulent eddy viscosity are plotted against the vessel's radius at u′=3.0 m/s and Φ = 1.0, as shown in Fig. 4. The mean turbulent kinetic energy balance has been conducted at u′=3.0 m/s rather than other turbulence intensities, to ensure the existence of HIT condition at the center of the vessel up to the maximum operating turbulence level.

It can be clearly noticed that both quantities reach their maximum value near the mixing fans (e.g., at higher turbulence intensities) and start to gradually decrease until reaching their minimum value at the center point of the vessel. Also, it can be observed that the value of these quantities remain almost constant up to a vessel radius of around 5 cm, which indicates that the turbulent flow field is homogeneous (e.g., the turbulent flow field is statistically independent of the coordinate system shift). In addition, the CFD turbulent kinetic energy contour implies that the turbulent flow field is isotropic (invariant to coordinate system reflections or rotation). The × and y velocity magnitudes were found to be similar in the central region of the vessel as shown in the CFD velocity contour, which further confirms the isotropy of the turbulent flow field. Furthermore, it can be observed from the plot in Fig. 4 that the turbulent eddy viscosity is close to zero at the vessel's central region, which indicates that the turbulence is uniform at the area of kernel development. Therefore, satisfying the HIT condition in the center of the vessel with a mean velocity($\overline{U}$ = zero < 0.1u′=1.35 m/s), which confirms that turbulence is not convicted, however it diffuses towards the vessel center

from the fan's region [67]. According to Ref. [59], it is important to determine the turbulent flame speeds at a flame radius (reference point) where the flame has left the ignition region and is only affected by a small portion of turbulent velocity field. Consequently, in this study, the turbulent flame speeds are computed at a flame radius that is equal to 6 cm.
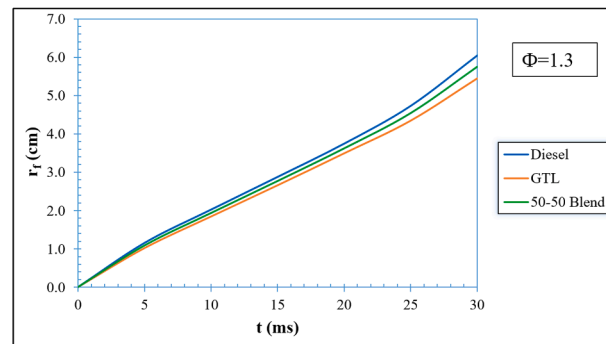
5.2. Flame radius evolution

A sequence of frames for the flame radius evolution of stoichiometric GTL-air mixture at 1 atm, and u =3.0 m/s is presented in Fig. 5. According to Zimont [24], the turbulent flame moves with a steady propagation velocity that depends on the mixture's physico-chemical properties and on the surrounding turbulence effect [26]. In addition, the averaged flame front is tracked out instead of the exact one. Upon averaging, a region with an instantaneous realization of the flame might be found, and it will be surrounding the mean flame front, and the region's width is known as the turbulent flame brush thickness δ$_t$. According to turbulent diffusion law [24], this model assumes an increasing thickness of the flame brush and a constant combustion velocity, and flames that follow this behavior are known as intermediate steady propagation (ISP) flames. It can be also noticed that the propagation rate increases as the flame grows and becomes closer to the fans region, because the developing kernel is subjected to an increasing spectrum of turbulence velocity scales. Prior to ignition, the turbulence was homogeneous and isotropic with an intensity level u =3.0 m/s, and a reaction progress C = 0 in all the vessel's domains. Just after ignition, the surface of the flame is relatively smooth (except of some distortions caused by the sparks) and it is "laminar like" [64]. As the flame develops, the surface of the flame becomes progressively wrinkled, on which the flame surface area, the flame thickness and the burning rate all increase. For the laminar cases (t < 25 ms), the flame radius develops linearly with time (e.g., flame acceleration is zero). However, for turbulent cases (t > 25 ms), the radius grows rapidly and non-linearly with time. In addition, the flame brush thickness is thickening as the flame develops, while having islands of burned gases inside it (C = 1 in CFD color bar) and islands of unburned gases outside it (C = 0 in CFD color bar) [50]. Therefore, spherically expanding flame vessels are used as a
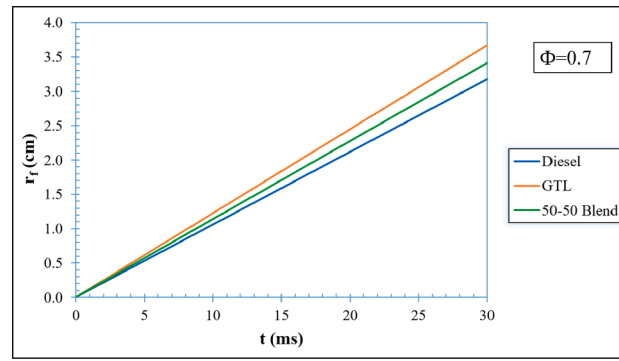
(a)
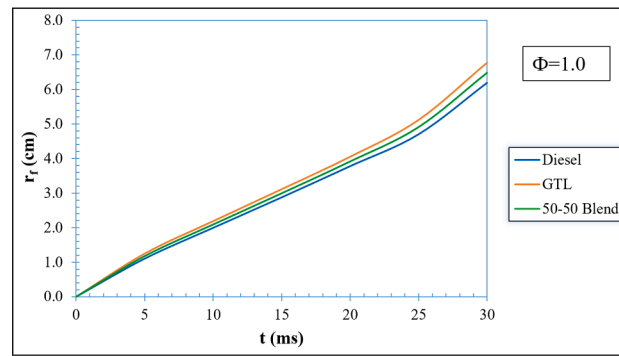
(b)

(c)

Fig. 6. Flame radius evolution for diesel, GTL, 50/50 diesel-GTL blend at, (a) $\Phi = 0.7$, (b) $\Phi = 1.0$, (c) $\Phi = 1.3$.

facility to provide turbulent flame speeds over a wide range of turbulence intensity levels by referring to the flame radius evolution history. According to Zimont TFC model [24], the mean flame front herein is assumed as a circle whose center is at the centroid of the flame. Similar trends for the flames radius evolutions were obtained at other equivalence ratio, however the propagation speeds were slightly different. Fig. 6 (a-c) compare between the flame radius evolution for diesel, GTL, 50/50 diesel-GTL blend at $\Phi = 0.7$, 1.0 and 1.3, respectively.

It can be clearly noticed from Fig. 6 (a-c) that the flame radius evolution for the lean mixtures ($\Phi = 0.7$) is the slowest, while the fastest radius evolution is depicted at the stoichiometric condition for all the fuels. According to Ref. [20], the unburned to burned density ratio ($\sigma = \rho_u / \rho_b$) has a monotonic behavior with the equivalence ratio, where the minimum value occurs at stoichiometric condition for all the fuels. In addition, the density ratio is higher for lean mixtures when compared to

fuel-rich cases. As σ decreases, the local burning rate for the stretched flamelets (portion of stretched laminar flame in a turbulent flow field) is enhanced significantly, which results in a faster flame radius evolution (and hence a higher burning velocity). As observed in Fig. 6(a), lean GTL fuel is characterized by the fastest flame radius development due to its lowest density ratio ($\sigma = 0.226$ for GTL, 0.229 for 50/50 diesel-GTL blend, and 0.232 for diesel). However, for the fuel rich case ($\Phi = 1.3$) in Fig. 6(c), diesel is characterized by the fastest flame development due to its lowest density ratio ($\sigma = 0.201$ for diesel, 0.206 for 50/50 diesel-GTL blend, and 0.210 for GTL). In all the three cases, it can be noticed that the 50/50 diesel-GTL blend exhibits an intermediate behavior between diesel and GTL fuels. In addition, it should be noticed how the behavior of the flame starts to change from linear (laminar) to nonlinear (turbulent), as the flame radius exceeds 5 cm.
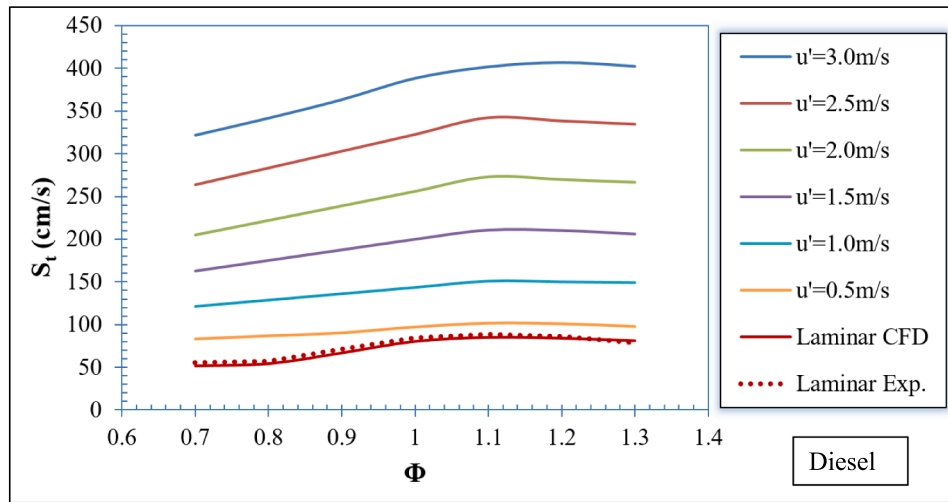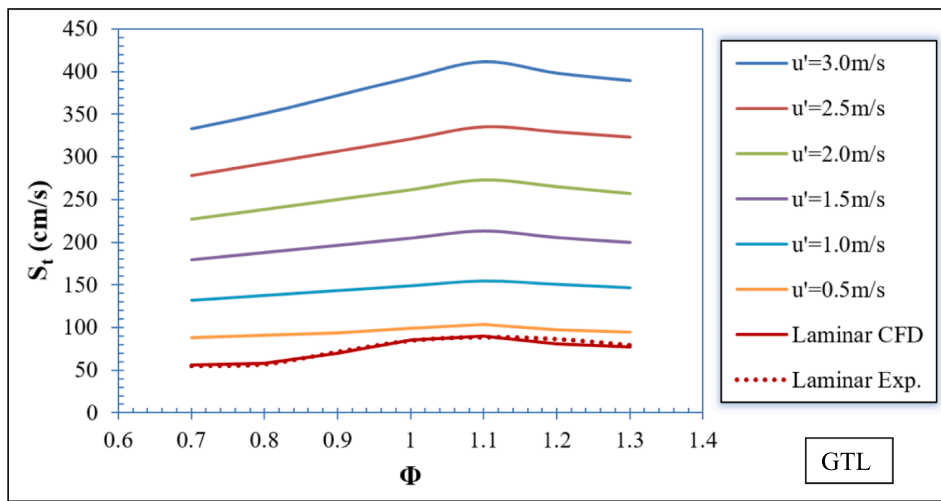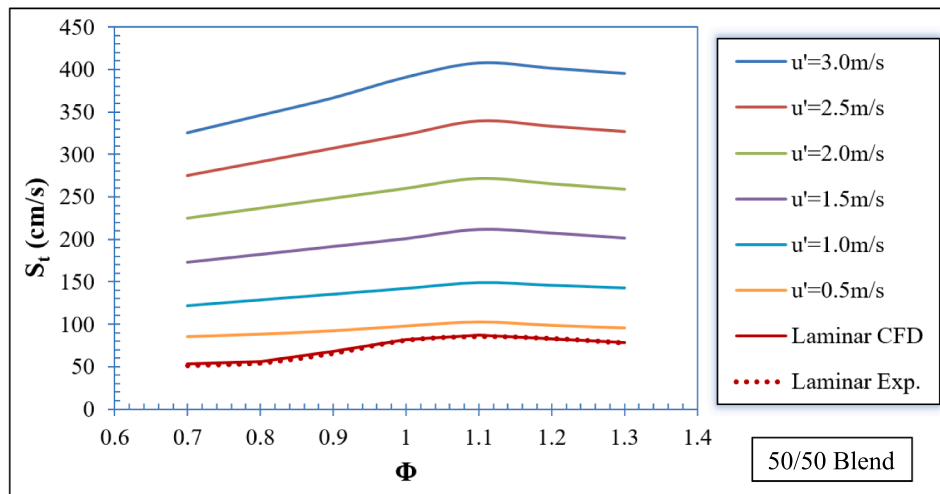
Fig. 7. Turbulent flame speeds vs. equivalence ratio at different turbulence intensities for, (a) diesel, (b) GTL, (c) 50/50 diesel-GTL blend. The experimental laminar flame speeds readings are obtained from [53].
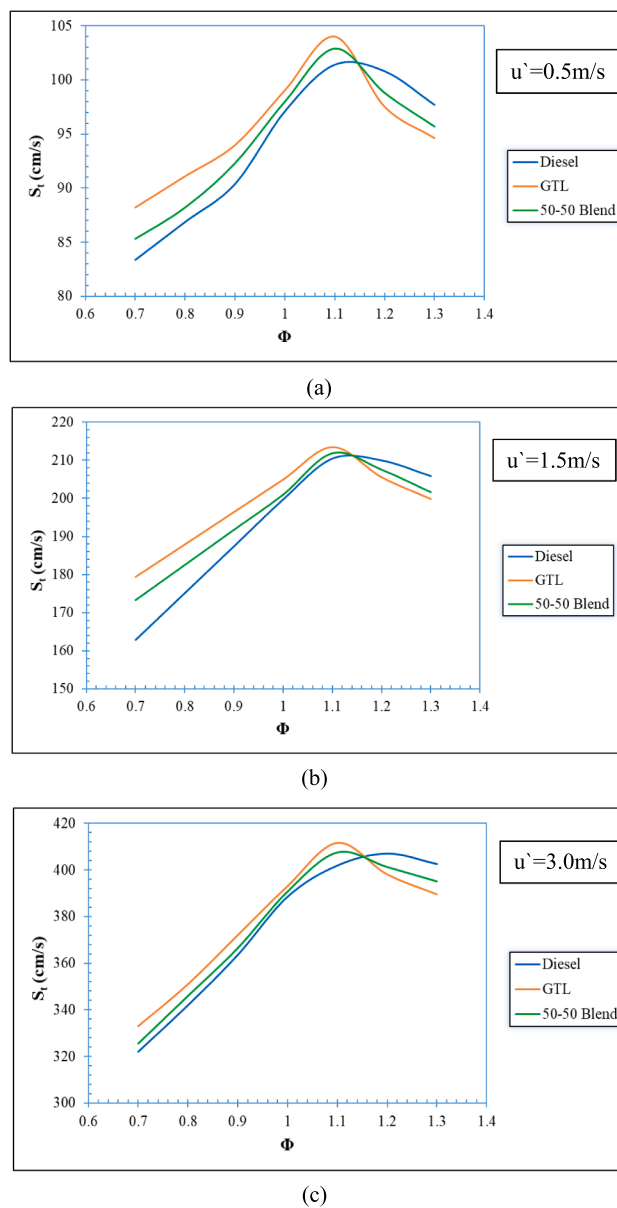
Fig. 8. Turbulent flame speeds vs. equivalence ratio for the three fuels at, (a) u'=0.5 m/s, (b) u'=1.5 m/s, (c) u'=3.0 m/s.

5.3. Turbulent flame Speeds, S_t

Turbulent flame speeds of the three liquid fuel blends were computed at different equivalence ratio (Ø=0.7 to 1.3) and turbulence intensities (u'=0.5 m/s to 3.0 m/s) as shown in Fig. 7 (a-c). In addition, the effect of varying the equivalence ratios on the turbulent flame speeds for the three hydrocarbon fuels is investigated at three different turbulence intensity levels, as illustrated in Fig. 8. Besides, the effect of blending diesel with GTL in a 50/50 fuel blend can be clearly noticed in Fig. 8. Furthermore, the laminar flame speeds were computed using the CFD solver with a laminar flame mode, and the numerical results were plotted versus the experimental ones [53].

It can be clearly noticed that the laminar flame speeds readings computed by CFD solver are remarkably close to the experimental ones, where the relative error percentage was found to be<4% at all the equivalence ratio. Third order least square fits were used to plot the turbulent flame speeds curves through each set of numerical data with a maximum standard deviation of ± 1.1 cm/s. As observed, all the curves

are "bell-shaped" where the laminar or turbulent flame speed peaks at near-stoichiometric condition (Ø=1.1), and falls when the mixture becomes leaner or richer. In addition, the gradual increase in the turbulence intensity level results in an increase in the turbulent flame speeds at all equivalence ratios. Fig. 8 (a-c) reveals the effect of varying the equivalence ratio on the turbulent flame speeds for the three hydrocarbon fuels at three different turbulence intensity levels (u'=0.5 m/s, u'=1.5 m/s and u'=3.0 m/s), respectively.

It can be clearly noticed how the increase in the turbulence intensity level causes a remarkable increase in the turbulent flame speeds for all the fuels. S_t increases roughly linearly with u'/S_l (low turbulence region), then levels off (bending region) and finally decreases again as it reaches the quenching limit [68]. Also, it can be noticed from Fig. 8 (a-c) that the turbulent flame speeds of lean GTL fuel are higher than lean diesel and lean 50/50 diesel-GTL blend, while diesel being the lowest. On contrast, rich diesel is characterized by a higher turbulent flame speed when compared to rich GTL and rich 50/50 diesel-GTL blend. These trends can be interpreted by the effect of Lewis number (Le) on the
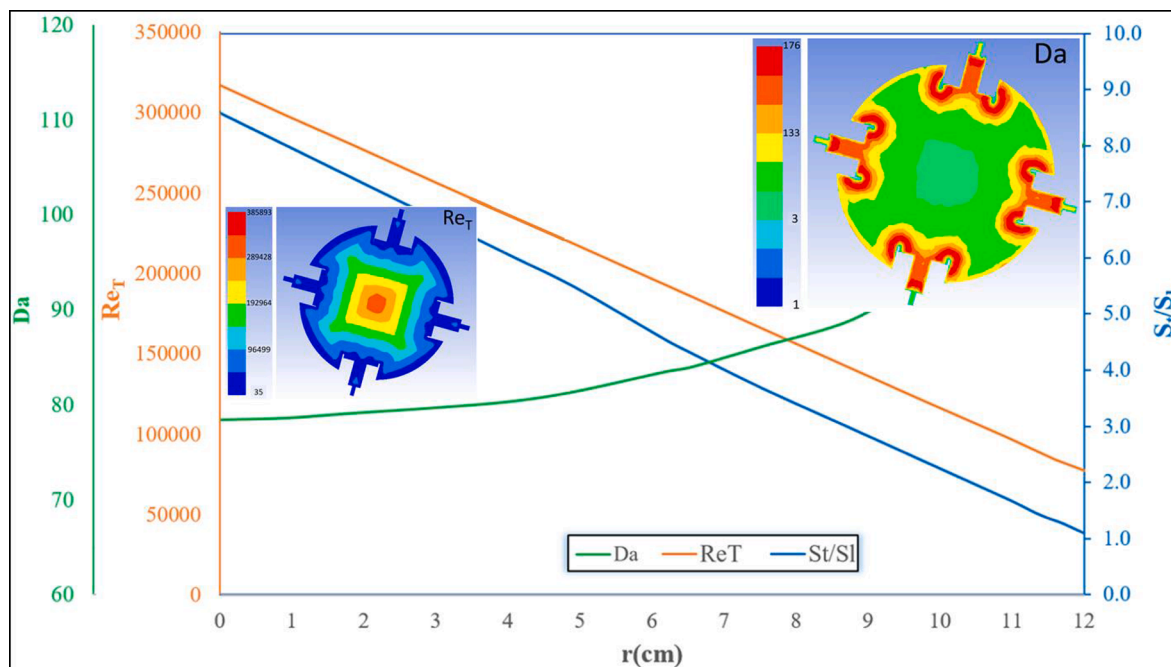
Fig. 9. The relation between the normalized turbulent flame speeds, turbulent Reynolds number and Damkohler number throughout the vessel radius ($0 < r < 12$ cm) for stoichiometric GTL at $u'=3.0$ m/s and $t = 30$ ms.

turbulent flame propagation. Lewis number defines the ratio between the mixture thermal diffusivity to its mass diffusivity [20]. Non-unity Lewis numbers can negatively affect or enhance the local burning rate. When $Le > 1$, the local burning rate is reduced (enhanced) due to the enhanced (reduced) heat loss in the positively curved segments [69]. When $Le < 1$, the mean curvature and mean strain rate become both positive at the flame front leading edge. Subsequently, the probability of finding positively curved, stretched flamelets (convex towards the direction of unburnt gas) becomes higher for premixed turbulent reacting flow. The laminar flamelets which are stretched by the action of turbulent eddies causes a considerable deviation in the local burning rate compared to the un-stretched laminar flame speed. Consequently, for mixtures with $Le < 1$, the turbulent flame speeds are augmented by an increase in the flamelet surface area, in addition to an increase in the local burning rate [20]. These impacts explain the higher turbulent flame speeds for lean GTL (or rich diesel) which are characterized by $Le < 1$ (values for Le are listed in Table 8). Similar trends have been also documented by [69–71]. In addition, it can be observed that the 50/50 diesel-GTL blend exhibits an intermediate behavior compared to pure liquid fuels, while maintaining the bell-shaped trend at different turbulence intensities. The addition of GTL to the pure conventional diesel with a 50% volumetric composition in the mixture caused around 3% increase in S_t at lean operating conditions.

5.4. Dimensionless numbers for turbulent combustion (Re_T, Da)

Reynolds number is an important dimensionless quantity used in fluid mechanics to define the ratio between inertial forces to viscous forces. Thus, a higher value of Re_T indicates for a higher level of turbulence [72]. On the other hand, Damkohler number is used in premixed turbulent combustion to define the ratio between the characteristic eddy time scale and chemical time scale [73]. Typically, S_t is proportional to Re_T and it is inversely proportional to Da. Fig. 9 shows the relation between the normalized turbulent flame speeds, turbulent Reynolds

number and Damkohler number throughout the vessel radius ($0 < r < 12$ cm) for stoichiometric GTL fuel at $u'=3.0$ m/s, and $t = 30$ ms.

It can be observed from Fig. 9 that Re_T peaks at the center of the vessel. This region is characterized by the lowest turbulent eddy viscosity and turbulent kinetic energy (as indicated in Fig. 4), which increases gradually until reaching its maximum value near the mixing fans. Subsequently, the peak value of Re_T is found at the center of the vessel. S_t/S_l is directly proportional to Re_T, and this attitude is consistent with the definition of this non-dimensional number, wherein, Re_T is directly proportional to u'/S_l. In addition, the results agree with the kinematic constraint, as $u' \to 0$ (which implies, $Re_T \to 0$), turbulent flame speeds should equal the laminar flame speeds (i.e., $S_t/S_l \to 1$). $Da > 1$ throughout the whole flame radius, which indicates that the chemistry has dominated the turbulence at all regions with different reaction rates and the flame is propagating towards the vessel's wall. S_t/S_l is inversely proportional to Da, and this attitude is consistent with the definition of this non-dimensional number, wherein, Da is inversely proportional to u'/S_l. Moreover, the data agrees with the kinematic constraint, as $u' \to 0$ (which implies, $Da \to \infty$), turbulent flame speeds should equal the laminar flame speeds (i.e., $S_t/S_l \to 1$) [20]. S_t/S_l has been plotted as a function of Re_T and Da for the three fuels at $t = 30$ ms, as illustrated in Fig. 10(a, b), respectively.

At the same elapsed time ($t = 30$ ms), Re_T and Da are greater for GTL fuel compared to diesel and 50/50 diesel-GTL blend. This gives an indication that the flame is propagating towards the vessel's wall at a faster rate in the case of using GTL fuel instead of other fuels. In addition, the flame radius evolution is quicker, and the chemistry has dominated turbulence in a shorter time for the case of GTL fuel compared to other fuels. These observations emphasis on the conclusions reached in Fig. 6 and Fig. 8, which have revealed that stoichiometric GTL fuel is characterized by a faster flame radius development and a higher turbulent flame speed, respectively.
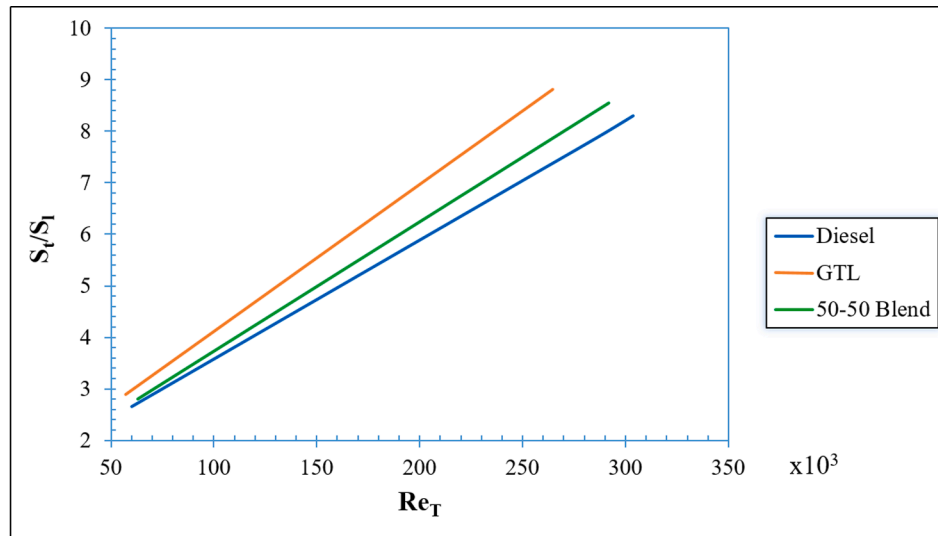
(a)
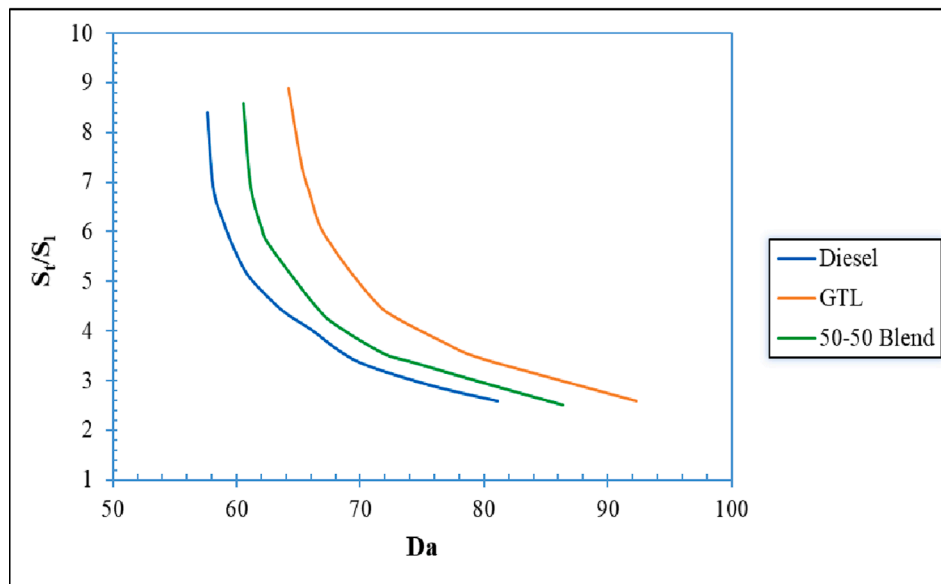
(b)

Fig. 10. a) S_t/S_l vs. Re_T, b) S_t/S_l vs. Da for the three fuels at u′=3.0 m/s, Ø=1.0 and t = 30 ms.

5.5. Borghi diagram

Borghi diagram is used in premixed turbulent combustion to indicate for the typical structure of the flame [74]. The flame morphologies for stoichiometric GTL fuel is determined at three different turbulence intensities, u′ = 0.5 m/s, u′ = 1.5 m/s and u′ = 3.0 m/s, as shown by Fig. 11.

At Ø = 1.0 and u′ = 0.5 m/s, the turbulence intensity is low, i.e., u′/S_l < 1, which leads to a wrinkled flamelet regime. Therefore, the reaction is confined by a highly wrinkled, thin interface that separates burned products from unburned reactants. Commonly, this structure is referred to as flamelets, which is assumed to have a local structure similar to that of a stretched laminar flame. For the other two cases (u′ = 1.5 m/s and u′ = 3.0 m/s), the turbulence intensity is higher than the laminar flame speed, i.e., u′/S_l > 1, and the flame structure is defined by

the corrugated flamelets regime. The role played by the laminar flamelet instabilities is reduced, and the combustion is influenced by turbulence, mainly by increasing the flamelet surface area [50].

6. Conclusions

Transient 3-D numerical investigations were performed to study turbulent flames of three liquid fuel blends (diesel, GTL, 50/50 diesel-GTL blend) using Zimont TFC model. The model is validated against the experimental work of Ravi [20]. The existence of HIT condition in the center of the vessel has been verified through studying turbulent kinetic energy balance throughout the vessel. The rate of flame radius evolution and turbulent flame speeds were found to be higher for lean GTL fuel compared to other fuels due to its lower density ratio and due to having a Le < 1. In contrast, rich diesel was found to have a faster flame
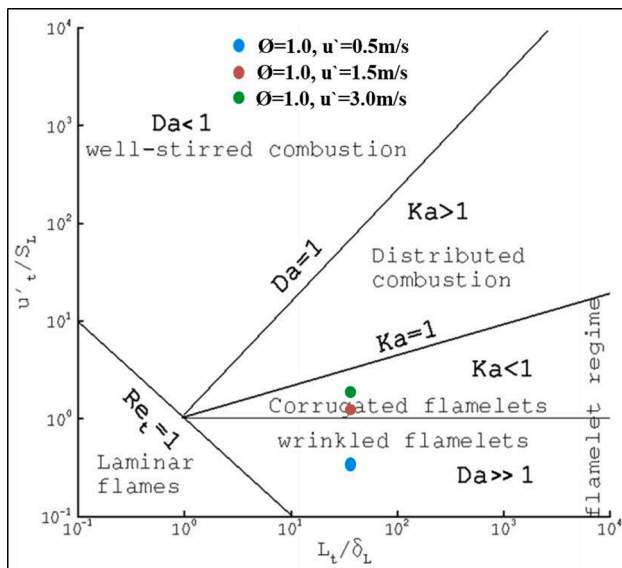
Fig. 11. Determination of combustion regime for stoichiometric GTL fuel on Borghi diagram at three different turbulence intensities, u′=0.5 m/s, u′=1.5 m/s and u′=3.0 m/s.

development and higher turbulent flame speeds due to the same reasons. In all cases, it was found that 50/50 diesel-GTL blend exhibits an intermediate behavior compared to other fuels. The normalized turbulent flame speeds were plotted against Reynolds number and Damkohler number for all the fuels at stoichiometric condition. At the same elapsed time (t = 30 ms), Re_T and Da were found to be greater for GTL fuel compared to diesel and 50/50 diesel-GTL blend, which indicates that the flame propagates towards the vessel's wall at a faster rate and the chemistry has dominated turbulence in a shorter time. Finally, the flame structure for stoichiometric GTL fuel has been studied at three different turbulence intensity levels (u′=0.5 m/s, u′=1.5 m/s and u′=3.0 m/s). At low turbulence level (u′=0.5 m/s), the flame morphology was defined by a wrinkled flamelet regime. However, at moderate and higher turbulence levels (u′=1.5 m/s and u′=3.0 m/s), the flame structure was defined by the corrugated flamelets regime.

CRediT authorship contribution statement

Abdellatif M. Sadeq: Software, Validation, Data curation. **Samer F. Ahmed:** Conceptualization, Supervision, Methodology, Formal analysis. **Ahmad K. Sleiti:** Project administration, Supervision, Methodology, Data curation.

Declaration of Competing Interest

The authors declare that they have no known competing financial interests or personal relationships that could have appeared to influence the work reported in this paper.

Acknowledgement

References

[1] Demirbas A. Progress and recent trends in biofuels. Prog Energy Combust Sci 2007; 33(1):1–18. https://doi.org/10.1016/j.pecs.2006.06.001.

[2] U. S. E. Information, "Annual Energy Outlook 2015 with projections to 2040," Off. Integr. Int. Energy Anal., vol. 1, pp. 1–244, 2015, DOE/EIA-0383(2013).

[3] Panwar NL, Kaushik SC, Kothari S. Role of renewable energy sources in environmental protection: A review. Renew Sustain Energy Rev 2011;15(3): 1513–24. https://doi.org/10.1016/j.rser.2010.11.037.

[4] Evans A, Strezov V, Evans TJ. Assessment of sustainability indicators for renewable energy technologies. Renew Sustain Energy Rev 2009;13(5):1082–8. https://doi. org/10.1016/j.rser.2008.03.008.

[5] Samim S, Sadeq AM, Ahmed SF. Measurements of Laminar Flame Speeds of Gas-to-Liquid-Diesel Fuel Blends. J Energy Resour Technol Trans ASME 2016;138(5):1–8. https://doi.org/10.1115/1.4033627.

[6] UNITED NATIONS, "PARIS AGREEMENT," pp. 1–25, 2015.

[7] K. Choi, S. Park, H. G. Roh, C. S. Lee, "Combustion and emission reduction characteristics of GTL-biodiesel fuel in a single-cylinder diesel engine," Energies, vol. 12, no. 11, 2019, 10.3390/en12112201.

[8] Shell Qatar, 2010, 'Pearl GTL, Overview'., 2010, 10.1016/j.aej.2016.06.026.

[9] A. M. Sadeq, M. A. Bassiony, A. M. Elbashir, S. F. Ahmed, M. Khraisheh, Combustion and emissions of a diesel engine utilizing novel intake manifold designs and running on alternative fuels, Fuel, vol. 255, no. July, 2019, 10.1016/j. fuel.2019.115769.

[10] Kianifar A, Ghafoorianfar N, Kianifar MR, Alam F. Numerical combustion modelling of a gas-burner. Int J Mech Mater Eng 2009;4(3):211–9.

[11] Galmiche B, Mazellier N, Halter F, Foucher F. Turbulence characterization of a high-pressure high-temperature fan-stirred combustion vessel using LDV, PIV and TR-PIV measurements. Exp Fluids 2014;55(1). https://doi.org/10.1007/s00348-013-1636-x.

[12] A. M. Sadiq, A. K. Sleiti, S. F. Ahmed, "Turbulent Flames in Enclosed Combustion Chambers: Characteristics and Visualization—A Review, J. Energy Resour Technol, 142, (8), 2020, 10.1115/1.4046460.

[13] Bradley D, et al. Turbulent burning velocity, burned gas distribution, and associated flame surface definition. Combust Flame 2003;133(4):415–30. https:// doi.org/10.1016/S0010-2180(03)00039-7.

[14] Bradley D, Lawes M, Morsy ME. Measurement of turbulence characteristics in a large scale fan-stirred spherical vessel. J Turbul 2019;20(3):195–213. https://doi. org/10.1080/14685248.2019.1610566.

[15] Griebel P, Siewert P, Jansohn P. Flame characteristics of turbulent lean premixed methane/air flames at high pressure: Turbulent flame speed and flame brush thickness. Proc Combust Inst 2007;31(II(2)):3083–90. https://doi.org/10.1016/j. proci.2006.07.042.

[16] A. M. Ruelas, E. L. Petersen, N. Donohoe, A. Heufer, "Laminar and Turbulent Flame Speeds for Natural Gas / Hydrogen Blends," no. June, 2014, 10.1115/GT2014-26742.

[17] Nguyen MT, Yu D, Chen C, Shy SS. General Correlations of Iso-octane Turbulent Burning Velocities Relevant to Spark Ignition Engines. Energies 2019;12:1848. https://doi.org/10.3390/en12101848.

[18] Mannaa O, et al. Turbulent burning characteristics of FACE-C gasoline and TPRF blend associated with the same RON at elevated pressures. Exp Therm Fluid Sci 2019;95:104–14. https://doi.org/10.1016/j.expthermflusci.2018.02.019.

[19] M. Lawes, R. Woolley, "Aspects of Laminar and Turbulent Burning Velocity Relevant to SI Engines," no. March, 2000, 10.4271/2000-01-0192.

[20] Ravi S. Measurement of Turbulent Flame Speeds of Hydrogen and Natural Gas Blends (C1–C5 Alkanes) Using a Newly Developed Fan-Stirred Vessel. Texas A&M 2014.

[21] Leuckel W, Nastoll W, Zarzalis N. Experimental Investigation of the Influence of turbulence on the Transient Premixed Flame Propagation Inside Closed Vessels. The Combustion Institute 1990;729–34.

[22] Fairweather M, Ibrahim SS, Jaggers H, Walker DG. Turbulent premixed flame propagation in a cylindrical vessel. Symp. (Int.) Combust. 1996;26(1):365–71. https://doi.org/10.1016/S0082-0784(96)80237-2.

[23] P. O. Ayegba, "Turbulence statistics and flow structure in fluid flow using particle image velocimetry technique : A review," no. August 2019, pp. 1–49, 2020, 10.1002/eng2.12138.

[24] Zimont VL. Theory of turbulent combustion of a homogeneous fuel mixture at high reynolds numbers. Combust Explos Shock Waves 1979;15(3):305–11. https://doi. org/10.1007/BF00785062.

[25] Zimont V, Polifke W, Bettelini M, Weisenstein W. An efficient computational model for premixed turbulent combustion at high reynolds numbers based on a turbulent flame speed closure. J Eng Gas Turbines Power 1998;120(3):526–32. https://doi. org/10.1115/1.2818178.

[26] V. L. Zimont, "Gas Premixed Combustion at High Turbulence . Turbulent Flame Closure Combustion Model .".

[27] Hawkes ER, Cant RS. Physical and numerical realizability requirements for flame surface density approaches to large-eddy and Reynolds averaged simulation of premixed turbulent combustion. Combust Theory Model 2001;5(4):699–720. https://doi.org/10.1088/1364-7830/5/4/310.

[28] Rasam A. "Explicit algebraic subgrid-scale stress and passive scalar flux modeling in large eddy simulation Amin. Rasam 2011.

[29] Bi M, Dong C, Zhou Y. Numerical simulation of premixed methane-air deflagration in large L/D closed pipes. Appl Therm Eng 2012;40:337–42. https://doi.org/ 10.1016/j.applthermaleng.2012.01.065.

[30] Biagioli F, Zimont VL. Gas dynamics Modelling of Counter gradient Transport in Open and Impinging Turbulent Premixed Flames. Proc Combust Inst 2002;29: 2087–95.

[31] Birkestad H. Separation and Compression of CO2 in an O2/CO2-fired Power Plant. CHALMERS 2002.

[32] Salaün E, et al. Experimental investigation of a spray swirled flame in gas turbine model combustor. In: in 18th International Symposium on the Application of Laser and Imaging Techniques to Fluid Mechanics; 2016. p. 1–23.

[33] Basidh, S. Gunasekar, and D. Devarasu, "Experimentation of Flame Stabilization Using Half V-Gutter Experimentation of Flame Stabilization Using Half V-Gutter,"

in Conference: 29th National Comvention of Aerospace Engineers $ National Seminar on Aerospace Engineering, 2015, no. November, pp. 1–9.

[34] Lipatnikov A, Chomiak J. Turbulent Burning Velocity and Speed of Developing, Turbulent Burning Velocity and Speed of Developing. Curved Strained Flames 2002;29:2113–21.

[35] Goulier J, Chaumeix N, Halter F, Meynet N, Bentaïb A. Experimental study of laminar and turbulent flame speed of a spherical flame in a fan-stirred closed vessel for hydrogen safety application. Nucl Eng Des 2017;312:214–27. https://doi.org/10.1016/j.nucengdes.2016.07.007.

[36] Habisreuther FZP, Bockhorn MHH. Modelling of a Premixed Swirl-stabilized Flame Using a Turbulent Flame Speed Closure Model in LES. Flow Turbul Combust 2009;82:537–51. https://doi.org/10.1007/s10494-008-9175-x.

[37] Palanti L, Pampaloni D, Andreini A, Facchini B. Numerical simulation of a swirl stabilized methane-air flame with an automatic meshing CFD solver. Energy Procedia 2018;148:376–83. https://doi.org/10.1016/j.egypro.2018.08.098.

[38] S. Yu, X. Liu, X. S. Bai, A. M. Elbaz, W. L. Roberts, "LES / PDF modeling of swirl-stabilized non-premixed methane / air flames with local extinction and re-ignition," vol. 219, pp. 102–119, 2020, Doi: 10.1016/j.combustflame.2020.05.018.

[39] A. Andreini, C. Bianchini, and A. Innocenti, "Large Eddy Simulation of a Bluff Body Stabilized Lean Premixed Flame," vol. 2014, 2014.

[40] Jones WP, Marquis AJ, Wang F. Large eddy simulation of a premixed propane turbulent bluff body flame using the Eulerian stochastic field method. Fuel 2015;140:514–25. https://doi.org/10.1016/j.fuel.2014.06.050.

[41] D. Huang, J. Xu, R. Chen, H. Meng, "Large eddy simulations of turbulent combustion of kerosene-air in a dual swirl gas turbine model combustor at high pressures, Fuel, vol. 282, no. July, p. 118820, 2020, 10.1016/j.fuel.2020.118820.

[42] Ahmed U, Prosser R. Modelling flame turbulence interaction in RANS simulation of premixed turbulent combustion. Combust Theory Model. 2016;20(1):34–57. https://doi.org/10.1080/13647830.2015.1115130.

[43] Salehi MM, Bushe WK. Presumed PDF modeling for RANS simulation of turbulent premixed flames. Combust. Theory Model 2010;14(3):381–403. https://doi.org/10.1080/13647830.2010.489957.

[44] Gövert S, Mira D, Kok JBW, Vazquez M, Houzeaux G. Turbulent Combustion Modelling of a Confined Premixed Methane/Air Jet Flame Using Tabulated Chemistry. Energy Procedia 2015;66:313–6. https://doi.org/10.1016/j.egypro.2015.02.070.

[45] Zimont VL, Battaglia V. Joint RANS/LES approach to premixed flame modelling in the context of the TFC combustion model. Flow Turbul Combust 2006;77(1–4): 305–31. https://doi.org/10.1007/s10494-006-9048-0.

[46] Ennetta R, Lajili M, Said R. Study of methane propagating flame characteristics using pdf - Monte Carlo model and reduced chemical kinetic scheme. Energy Fuels 2009;23(6):2903–7. https://doi.org/10.1021/ef9000456.

[47] Wang Q, Ma H, Shen Z, Guo Z. Numerical simulation of premixed methane-air flame propagating parameters in square tube with different solid obstacles. Procedia Eng 2013;62:397–403. https://doi.org/10.1016/j.proeng.2013.08.081.

[48] H. Deng, M. Huang, X. Wen, G. Chen, F. Wang, Z. Yao, "Numerical investigation of premixed methane-air flame in two-dimensional half open tube in the early stages," Fuel, vol. 272, no. March, p. 117709, 2020, 10.1016/j.fuel.2020.117709.

[49] B. Bazooyar and H. Gohari Darabkhani, "Analysis of flame stabilization to a thermo-photovoltaic micro-combustor step in turbulent premixed hydrogen flame," Fuel, vol. 257, no. March, p. 115989, 2019, 10.1016/j.fuel.2019.115989.

[50] Thattai A. A Validation Study For Turbulent Premixed Flame Propagation In Closed Vessels Submitted in Partial Fulfillment. Delft University of Technology; 2010.

[51] Sleiti AK, Kapat JS. Comparison between EVM and RSM turbulence models in predicting flow and heat transfer in rib-roughened channels. J Turbul 2006;7. https://doi.org/10.1080/14685240500499343.

[52] Zimont VL. A numerical model of premixed turbulent combustion of gases. Chem Phys Reports 2017;14(7):993–1025.

[53] Samim S. Investigation of Laminar Flame Speed of Alternative Liquid Fuel Blends. Qatar University; 2016.

[54] T. D. Canonsburg, ANSYS Fluent Tutorial Guide, vol. 15317, no. November. 2013.

[55] ANSYS Fluent Tutorial Guide 18, "ANSYS Fluent Tutorial Guide 18," ANSYS Fluent Tutor. Guid. 18, vol. 15317, no. April, pp. 724–746, 2018.

[56] Alawadhi EM. "Meshing guide" 2020. https://doi.org/10.1201/b18949-12.

[57] S. S. Shy, W. K. I, M. L. Lin, "A new cruciform burner and its turbulence measurements for premixed turbulent combustion study," Exp Therm Fluid Sci 20, (3–4), pp. 105–114, 2000, 10.1016/S0894-1777(99)00035-7.

[58] Bradley D, Lawes M, Mansour MS. Correlation of turbulent burning velocities of ethanol-air, measured in a fan-stirred bomb up to 1.2MPa. Combust Flame 2011; 158(1):123–38. https://doi.org/10.1016/j.combustflame.2010.08.001.

[59] Ayache A. Experimental Measurement of Turbulent Burning Velocity of Premixed Biogas Flame. The University of Manitoba; 2017.

[60] Almansour B. Experimental Investigation of Advanced Ignition Systems for High Efficiency Combustion. University of Central Florida; 2019.

[61] "A Chemical Equilibrium Program for Windows." http://www.gaseq.co.uk/.

[62] "CHEMKIN-PRO (x64) 4.5," 2011. https://chemkin-pro-x64.software.informer. com/4.5/.

[63] J. W. Gooch, "Premix," 2011. 10.1007/978-1-4419-6247-8_9395.

[64] Morones A, et al. Laminar and turbulent flame speeds for natural gas/hydrogen blends. Proc ASME Turbo Expo 2015;4B(January):2014. https://doi.org/10.1115/GT2014-26742.

[65] Saw EW, et al. Experimental characterization of extreme events of inertial dissipation in a turbulent swirling flow. Nat Commun 2016;7:1–8. https://doi.org/10.1038/ncomms12466.

[66] Bonhomme A, Duchaine F, Wang G, Selle L, Poinsot T. A parallel multidomain strategy to compute turbulent flows in fan-stirred closed vessels. Comput Fluids 2014;101:183–93. https://doi.org/10.1016/j.compfluid.2014.06.010.

[67] Choi SK, Kim SO. Turbulence modeling of natural convection in enclosures: A review. J Mech Sci Technol 2012;26(1):283–97. https://doi.org/10.1007/s12206-011-1037-0.

[68] Fru G, Thévenin D, Janiga G. Impact of turbulence intensity and equivalence ratio on the burning rate of premixed methane-air flames. Energies 2011;4(6):878–93. https://doi.org/10.3390/en4060878.

[69] Chen Z, Gou X, Ju Y. Studies on the outwardly and inwardly propagating spherical flames with radiative loss. Combust Sci Technol 2010;182(2):124–42. https://doi.org/10.1080/00102200903299850.

[70] Weiß M, Zarzalis N, Suntz R. Experimental study of Markstein number effects on laminar flamelet velocity in turbulent premixed flames. Combust Flame 2008;154 (4):671–91. https://doi.org/10.1016/j.combustflame.2008.06.011.

[71] Kido H, Nakahara M, Nakashima K, Hashimoto J. Influence of local flame displacement velocity on turbulent burning velocity. Proc Combust Inst 2002;29 (2):1855–61. https://doi.org/10.1016/S1540-7489(02)80225-5.

[72] I. L. A. Sequeira, "The Reynolds Number - Units in a Dimensionless Number The Reynolds Number - Units in a Dimensionless Number," in PDH online Course M476, vol. 476, 2013, pp. 1–27.

[73] Bak HS, Lee SR, Chen JH, Yoo CS. A numerical study of the diffusive-thermal instability of opposed nonpremixed tubular flames. Combust Flame 2015;162(12): 4612–21. https://doi.org/10.1016/j.combustflame.2015.09.019.

[74] Poinsot T, Veynante D, Candel S. Diagrams of premixed turbulent combustion based on direct simulation. Symp Combust 1991;23(1):613–9. https://doi.org/10.1016/S0082-0784(06)80308-5.